Quantum phase transitions in the $S=\frac{1}{2}$ distorted diamond chain

Yan-Chao Li and Shu-Shen Li
State Key Laboratory for Superlattices and Microstructures, Institute of Semiconductors, Chinese Academy of Sciences, P.O. Box 912, Beijing 100083, People's Republic of China
(Received 5 June 2008; published 13 November 2008)

By means of the second derivative of the ground-state and first-excited energy, the quantum phase transitions (QPTs) for the distorted diamond chain (DDC) with ferromagnetic and antiferromagnetic frustrated interactions and the trimerized case are investigated, respectively. Our results show the plentiful quantum phases owing to the spin interaction competitions in the model. Meanwhile, by using the transfer-matrix renormalization-group technique, we study the two-site thermal entanglement of the DDC model in the thermodynamic limit for a further understanding of the QPTs.

DOI: 10.1103/PhysRevB.78.184412 PACS number(s): 75.10.Pq, 64.60.−i, 03.65.Vf, 03.65.Ud

I. INTRODUCTION

Quantum phase transitions (QPTs) (Ref. 1) driven by small variations of external parameters, such as external magnetic field and press, occupy a significant position in quantum many-body systems. Studying them can provide a better understanding to exploit the unusual properties of these materials, for instance, the decoherence and entanglement problems in the field of quantum computation, especially at finite temperatures. Furthermore, it also helps us find new functional materials, such as high-temperature superconductors and novel semiconductors.[2–4] The finding of magnetically mediated superconductivity in a heavy-fermion system, for example, shows a tight connection between quantum phase and properties of materials, which extremely enhanced people's interest in QPTs investigation.[4]

In recent years, a great deal of attention has been paid to QPTs study from the perspective of quantum information theory. Within such framework, one important concept in detecting QPTs is that of quantum entanglement, which captures information of a QPT through quantifying the strength of quantum correlations between subsystems of a many-body system.[5–11] More recently, another concept also borrowed from the field of quantum information science, quantum fidelity (QF), has been extensively exploited to characterize QPTs. Its initial definition is the overlap between two ground states corresponding to two slightly different parameters. Because different quantum states usually have distinct geometrical structure in Hilbert space of the system, the QF is able to capture the structural changing information when undergoing a QPT, thereby reflecting critical behavior.[12] Being purely a Hilbert-space geometrical quantity, no prior knowledge of the order parameter and the symmetry of the system is needed for the quantum fidelity method and it is expected to be a universal tool to investigate QPTs.[12,16] Considerable works based on this idea have been performed to investigate the role of fidelity (and its second derivative, i.e., the fidelity susceptibility) in characterizing QPTs of various quantum many-body systems,[12–19] such as the Dicke and spin models,[12–15] fermionic systems,[16,17] and the Bose-Hubbard model and the so-called matrix product states.[18,19]

There is a relative more complex spin model: the distorted diamond-chain (DDC) model. Due to its triangularlike spin arrangement, as shown in Fig. 1, competitions of interactions among spins would result in rich physical properties. It is regarded as an ideal model to investigate the magnetic frustrated phenomena[20–22] and has been wildly studied in condensed-matter physics. However, most works, both in the experiment and the theory, only focus on the thermodynamic or the magnetic properties of the system, such as the magnetic susceptibility as a function of temperature, the low-temperature specific heat, and the 1/3 magnetization plateau problems.[21–29]

Studies on the phase diagram of the DDC model, on the other hand, are relatively few. A so-called diamond-chain model, i.e., $J_1=J_2$ in Fig. 1, was first investigated by Takano *et al.*[30] They indicated that there exist three phases in the ground state (GS) of the diamond chain: the ferrimagnetic phase for $J_3/J_1<0.909$, the tetramer-dimer (TD) singlet phase for $0.909<J_3/J_1<2$, and the dimer-monomer (DM) phase for $J_3/J_1>2$. By using an analytical method as well as a so-called level spectroscopy analysis approach, Okamoto *et al.*[31–34] calculated the antiferromagnetic (AF) frustrated DDC model (with all the interactions among spins being AF) and showed that the DDC model possesses three phases: the ferrimagnetic (ferri), dimer (D), and spin fluid (SF) phases.

However, even these works only focused on the antiferromagnetic frustrated DDC model and only performed on finite-size systems, usually no more than 24 sites. Therefore, in this paper—by means of the fidelity approach—we aim to study the QPTs of the more generalized DDC model not only with antiferromagnetic frustrated interactions $(J_1,J_2,J_3>0)$ but also with ferromagnetic (F) frustrated interactions $(J_1,J_2<0$ and $J_3>0)$. Moreover, by using the transfer-matrix renormalization-group (TMRG) technique,[35,36] we

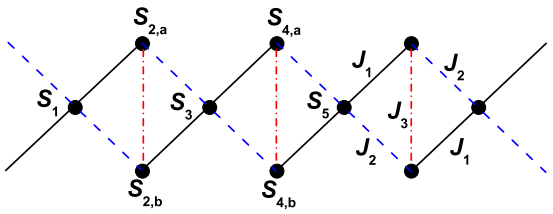

FIG. 1. (Color online) The spin-1/2 diamond-chain model. Black dots represent spin-1/2 coupled with exchange constants J_1, J_2, and J_3 indicated by the connecting lines.

calculate the thermal entanglement E_t to investigate the signatures of several QPTs of the system in the thermodynamical limit at finite temperatures.

This paper is organized as follows. In Sec. II, we first briefly introduce the DDC chain model and the definition of the quantum fidelity and then give an outline about the related methods we used. In Sec. III, we present the global phase diagram for the frustrated case and the trimerized case of the system by using the exact diagonalization technique. The two-site thermal entanglement E_t in the thermodynamic limit is calculated to analyze the signature of several QPTs at finite temperature by using the TMRG method in Sec. IV. Finally, in Sec. V, a brief summary is given.

II. MODEL AND METHODS

We first review the definition of the quantum fidelity. A general Hamiltonian of a quantum system undergoing a QPT can be written as

$$H(\lambda) = H_0 + \lambda H_1, \tag{1}$$

where H_1 is the driving term and parameter λ describes the intensity of a certain kind of interaction. When the parameter λ has a sight change δ ($|\delta| \ll 1$), the Hamiltonian of the system becomes $H(\lambda+\delta)=H(\lambda)+\delta H_1$. Then the quantum GS fidelity is defined as

$$F(\lambda, \delta) = |\langle \psi_0(\lambda) | \psi_0(\lambda + \delta) \rangle|, \tag{2}$$

where $\psi_0(\lambda)$ and $\psi_0(\lambda+\delta)$ are the two ground states of $H(\lambda)$ and $H(\lambda+\delta)$, respectively.[12] It marks QPTs by presenting the distinguishability of the two ground-state geometrical structure in the Hilbert space. However, the fidelity is dependent on δ. To exclude the influence coming from δ, You *et al.*[16,17] put forward the fidelity susceptibility (FS) from the perspective of quantum perturbation theory as

$$F_s(\lambda) = \sum_{n \neq 0} \frac{|\langle \psi_n(\lambda) | H_1 | \psi_0(\lambda) \rangle|^2}{[E_n(\lambda) - E_0(\lambda)]^2}, \tag{3}$$

where $|\psi_n(\lambda)\rangle$ and E_n are the eigenstates and eigenvalues of $H(\lambda)$, respectively. When the fidelity is expanded to the lowest order in δ, the coefficient of δ^2 actually defines the fidelity susceptibility. It is δ independent and sometimes a more effective tool to detect QPTs.

In fact, in terms of quantum perturbation theory [consider δ a perturbation to $H(\lambda)$], the GS energy of $H(\lambda)$ to the second order can be written as

$$E_0(\lambda + \delta) = E_0(\lambda) + \delta \langle \psi_0(\lambda) | H_1 | \psi_0(\lambda) \rangle + \delta^2 \sum_{n \neq 0} \frac{|\langle \psi_n(\lambda) | H_1 | \psi_0(\lambda) \rangle|^2}{E_0(\lambda) - E_n(\lambda)}. \tag{4}$$

If the second λ derivative of E_0 at $\delta=0$ is taken then we have

$$\left. \frac{\partial^2 E_0(\lambda)}{\partial \lambda^2} \right|_{\delta=0} = \sum_{n \neq 0} \frac{2|\langle \psi_n(\lambda) | H_1 | \psi_0(\lambda) \rangle|^2}{E_0(\lambda) - E_n(\lambda)}. \tag{5}$$

This result is consistent with the conclusion of Ref. 15, where the authors got the same equation from the Hellmann-Feynman theorem. It is clear that the FS and the second derivative of GS energy (SDGE) have the same physical origin as can be seen from Eqs. (3) and (5) and it has been proved that they play equivalent role in identifying QPT.[15] Because only the GS energy of the system is needed in Eq. (5), the SDGE approach is quite convenient to perform.

However, most models cannot be solved analytically. We could only obtain their numerical exact solutions for a small-size system, such as the DDC model. Because of finite-size effect and lack of size scaling analysis, it is difficult to identify QPTs for some cases. In Ref. 28, the authors used the so-called thermal pairwise concurrence to study the QPTs of the DDC model driven by the external magnetic fields in the thermodynamic limit. To solve the finite-size effect problem and verify some conclusions of our SDGE results, we calculate the two-site thermal entanglement E_t, i.e., the von Neumann entropy at finite temperature, for the DDC model without external magnetic field to investigate QPTs in the thermodynamical limit by using the TMRG method. This method is based on a Trotter-Suzuki decomposition of the partition function of a system, which maps a d-dimensional quantum system to a $d+1$-dimensional classical one; therefore it can directly handle infinite spin chains (for an overview, see Ref. 36).

The two-site thermal entanglement E_t can be achieved from the neighboring two-site reduced density matrix at sites i and j ($\rho_{i,j}$) of the system. $\rho_{i,j}$ can be obtained from the ground states of the system at finite temperature which correspond to thermodynamical average values. In the standard basis $\{|\uparrow\uparrow\rangle, |\uparrow\downarrow\rangle, |\downarrow\uparrow\rangle, |\downarrow\downarrow\rangle\}$, it can be written as

$$\rho_{i,j} = \begin{pmatrix} \langle P_i^{\uparrow} P_j^{\uparrow} \rangle & \langle P_i^{\uparrow} \sigma_j^{-} \rangle & \langle \sigma_i^{-} P_j^{\uparrow} \rangle & \langle \sigma_i^{-} \sigma_j^{-} \rangle \\ \langle P_i^{\uparrow} \sigma_j^{+} \rangle & \langle P_i^{\uparrow} P_j^{\downarrow} \rangle & \langle \sigma_i^{-} \sigma_j^{+} \rangle & \langle \sigma_i^{-} P_j^{\downarrow} \rangle \\ \langle \sigma_i^{+} P_j^{\uparrow} \rangle & \langle \sigma_i^{+} \sigma_j^{-} \rangle & \langle P_i^{\downarrow} P_j^{\uparrow} \rangle & \langle P_i^{\downarrow} \sigma_j^{-} \rangle \\ \langle \sigma_i^{+} \sigma_j^{+} \rangle & \langle \sigma_i^{+} P_j^{\downarrow} \rangle & \langle P_i^{\downarrow} \sigma_j^{+} \rangle & \langle P_i^{\downarrow} P_j^{\downarrow} \rangle \end{pmatrix}, \tag{6}$$

where $P^{\uparrow}=\frac{1}{2}(1+\sigma^z)$, $P^{\downarrow}=\frac{1}{2}(1-\sigma^z)$, and $\sigma^{\pm}=\frac{1}{2}(\sigma^x \pm i\sigma^y)$, The brackets denote ground-state expectation values and σ are the Pauli matrices.[37] The elements of the matrix is nothing but the thermal average of the product of P and σ. In TMRG calculations, the thermal average of an arbitrary local operator $A_{i,i+1}$ at two nearest sites can be easily calculated.[36] Thus, we can obtain the two-site reduced density matrix $\rho_{i,j}$ and E_t, where $E_t=-\mathrm{Tr}[\rho_{i,j} \log_2(\rho_{i,j})]$.

The spin-1/2 distorted diamond chain can be considered as a one-dimensional Heisenberg spin system. Its Hamiltonian is expressed as

$$H = \sum_{i=1}^{N} J_1 (\boldsymbol{S}_{2i-1} \cdot \boldsymbol{S}_{2i,a} + \boldsymbol{S}_{2i,b} \cdot \boldsymbol{S}_{2i+1}) + J_2 (\boldsymbol{S}_{2i-1} \cdot \boldsymbol{S}_{2i,b} + \boldsymbol{S}_{2i,a} \cdot \boldsymbol{S}_{2i+1}) + J_3 \boldsymbol{S}_{2i,a} \cdot \boldsymbol{S}_{2i,b}, \tag{7}$$

where $\boldsymbol{S}_i$ are spin=1/2 operators at site i, J_i with $i=1,2,3$ are exchange integrals ($J_i>0$ corresponds to antiferromagnetic interaction J_{AF}, while $J_i<0$ corresponds to ferromagnetic interaction J_F). In the following, we take $J_2=1$ as the energy unit.

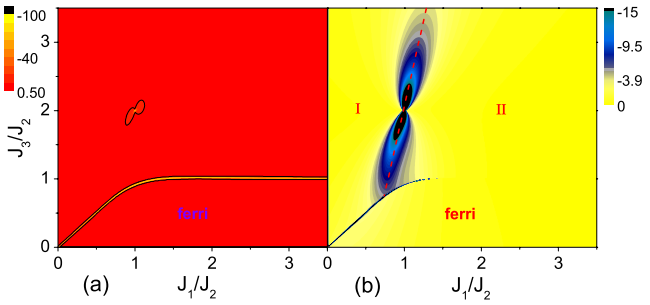

FIG. 2. (Color online) Contour map of the SDGE of the antiferromagnetic frustrated DDC model for $N=12$ on the J_1-J_3 plane with respect to (a) J_3 and (b) J_1. The red dashed line in (b) is guide for the eyes

In Sec. III, the Hamiltonian is diagonalized by using the exact diagonalization method for the SDGE and the second derivative of the first-excited energy (SDFE) results. The numerical error during the diagonalization is less than 1×10^{-14}. For the TMRG calculations in Sec. IV, we choose the two neighboring sites connected by J_1 (see Fig. 1) as the two sites for the calculation of $\rho_{i,j}$; the width of the imaginary time slice is taken as $\varepsilon=0.1$. At low temperature, the basis truncation error is important. We take $m=110$ states for the antiferromagnetic case and $m=100$ states for the other cases during the calculations for accuracy. The Trotter-Suzuki error is less than 1×10^{-3} and the truncation error is smaller than 1×10^{-8}.

III. GLOBAL PHASE DIAGRAM OF THE DDC MODEL

A. Frustrated case

We first calculate the SDGE of the DDC model with antiferromagnetic frustrated interactions to identify its QPTs by using the exact diagonalization technique with periodic boundary conditions. The contour map of the SDGE with respect to J_3 in the J_1-J_3 plane for $N=12$ and $\delta J_3=0.01$ is plotted in Fig. 2. The figure is separated into two main parts by a curve which corresponds to the dramatic drops of the SDGE. Comparing with the results in Ref. 31, we can conclude that the two parts are the ferrimagnetic and SF phases, respectively, as shown in Fig. 2. Except the ferri-SF phase-transition curve, there is also a sharp drop of the SDGE at around $J_1=1.0$ and $J_3=2.0$, which is shown as a dot in Fig. 2(a). This dot identifies the TD-DM phase transition, which is consistent with the reported value in Ref. 30.

Figure 2(b) shows the SDGE with respect to J_1 ($\delta J_1=0.01$) for the same conditions. Because the derivation is along the J_1 direction, the ferri-SF phase transition at the large vale J_1 part, which is parallel to the J_1 direction, is not presented. In this figure, besides the phase-transition point between tetramer-dimer and dimer-monomer phases, there are also minima around the red dashed line (a guide for the eyes), which separate the diagram, except of the ferrimagnetic phase region, into parts I and II. Could these minima be regarded as precursors of QPTs or are they just results of finite-size effect? We calculate the SDGEs with respect to J_1 for different system sizes N as plotted in Fig. 3. The minimum decreases as N increases. It seems that some kind of scaling behavior exists. But because the system size that we can calculate is too small, we cannot demonstrate the scaling behaviors clearly. Thus, we will use the TMRG method to have a further study in later part of the paper.

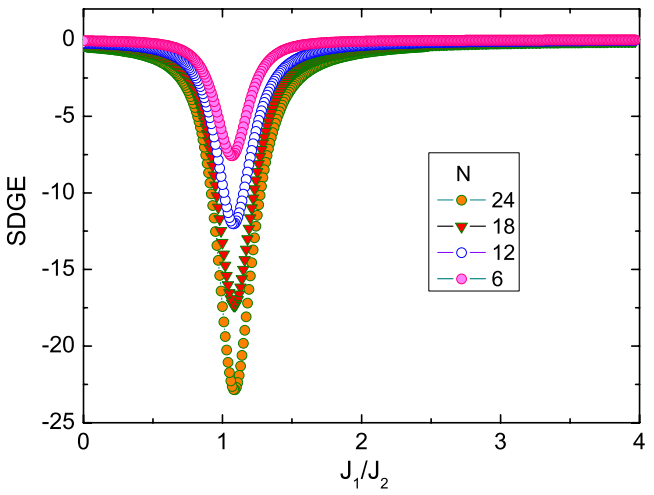

FIG. 3. (Color online) SDGE of the antiferromagnetic frustrated DDC model as a function of J_1/J_2 for different system sizes N at $J_3/J_2=2.5$.

One may note that the dimer phase pointed out in Ref. 31 does not appear in our SDGE calculated results (see Fig. 2). To make this problem clear, let us first look at the general characters of QPTs. It is known that QPTs can be divided into two main types: the first-order QPT (1QPTs) and the continuous QPT. The 1QPTs, which are caused by the GS energy crossing, can be characterized by discontinuities in the first derivative of the GS energy, such as the F-SF phase transition in the DDC model; while the second-order QPTs (2QPTs), which are caused by the limiting case of the so-called "avoided level crossing" in the thermodynamic limit, are usually characterized by discontinuities of the second derivative of the GS energy, such as the phase transition in the Ising model. The SF-D phase transition is known to be of Berezinskii-Kosterlitz-Thouless (BKT) type,[38,39] which belongs to the 2QPT. Thus, one may expect a sharp drop in the vicinity of the phase-transition point. However, we cannot find an extremal point in the SDGE results for a finite-size system. In fact, it has been proven in Ref. 40 that all the nth order derivatives of GS energy are continuous near the BKT-type phase critical point of the XXZ model even in the thermodynamic limit. To understand the unusual phenomenon, we shall return to Eq. (5). That Eq. (5) can be used to identify QPTs is due to the singularity caused by the vanishing energy gap in the thermodynamic limit. But a divergence may be absent when the matrix elements H^1_{n0} in Eq. (5) also vanish simultaneously as the energy gap tends to zero in the thermodynamic limit, as pointed out in Ref. 15; therefore the SDGE would fail to identify the QPT in this case.

In Ref. 14, the authors pointed out that the BKT-type QPTs can be well characterized by the fidelity between the first-excited states instead of the GS fidelity. Motivated by this, we calculate the second derivative of the first-excited energy of the DDC model. The contour map of the SDFE on

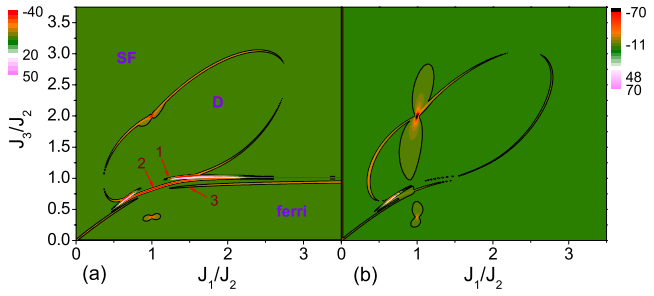

FIG. 4. (Color online) Contour map of the SDFE of the antiferromagnetic frustrated DDC model for $N=12$ on the J_1-J_3 plane with respect to (a) J_3 and (b) J_1.

the J_1-J_3 plane is plotted in Fig. 4, where the SF-D phase-transition critical points are clearly marked by the sharp drops of the SDFE. The boundary of the dimer phase seems to be consistent with the results in Ref. 31. To clarify this point, we consider a specific critical point at $J_3/J_2=0.8$ for $N=12$. The calculated results show that the dramatic drop point of the SDFE is $J_1/J_2=0.3752634$, which is consistent with the value 0.375263 given in Ref. 31. Meanwhile, the position of the extremum scales as $J_1^c(N) \simeq x_{J_3}/N^2+\text{const}$, where x_{J_3}, which is different for different J_3/J_2, denotes the slope coefficient of the curve and the extrapolation to the thermodynamic limit for $J_3/J_2=0.8$ shows that the critical point tends to be the same value with Ref. 31 ($J_1^c/J_2=0.352$) [see Fig. 5(a)]. We also give the scaling behavior of the positions of the extrema of the SDFE for $J_3/J_2=2.5$ as shown in Fig. 5(b). Now, we can say that the SDFE indeed can be used to characterize BKT-type QPT in the DDC model.

However, we find that the absolute value of the extremum decreases as the system size increases as shown in Fig. 6. This behavior is quite different from those of the GS fidelity or the SDGE in characterizing QPTs, where the absolute value of extremum increases with the increase of system size and diverges in the thermodynamic limit. To understand these phenomena, we must get further insight to the physical properties of the SF-D phase transition. It is known that the

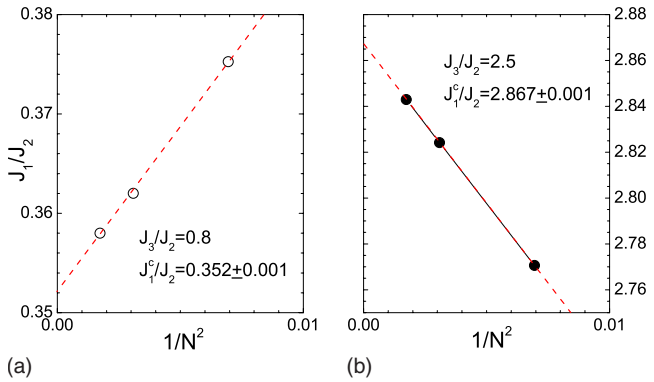

FIG. 5. (Color online) The extrapolation of J_1^c/J_2 to $N\to\infty$ for (a) the $J_3/J_2=0.8$ case and (b) the $J_3/J_2=2.5$ case. It shows that $J_1^c/J_2=0.352\pm0.001$ for the $J_3/J_2=0.8$ case and 2.867 ± 0.001 for the $J_3/J_2=2.5$ case, respectively. Here, the numerical error is less than 1×10^{-4} The red dashed lines are guides for the eyes.

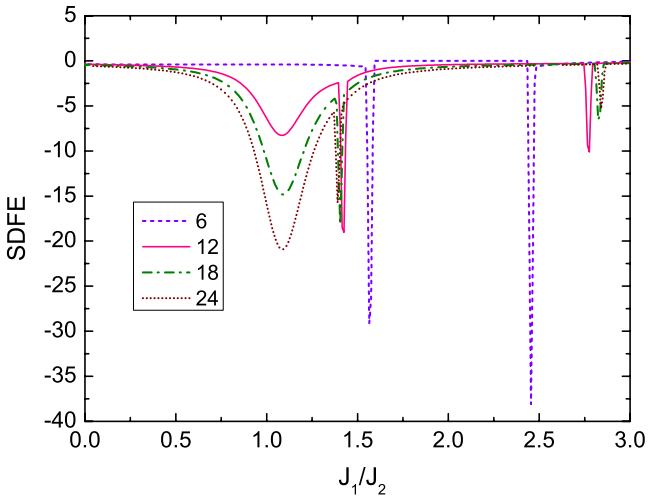

FIG. 6. (Color online) SDFE of the DDC model with respect to J_1 for different system sizes N at $J_3/J_2=2.5$. The sharp drops indicate the SF-D phase transition, whose absolute values decrease as the system size increases. The deep around $J_1/J_2=1.0$ corresponds to the one of the SDGE in Fig. 3.

D state is a spin-gapped state, while the SF state is spin gapless. For a finite system, the D state and the SF state have the same nondegenerate ground state with $S^z_{\text{total}}=0$; whereas their lowest excited states are quite different—a singlet lowest excited state with $S^z_{\text{total}}=0$ for the D phase, but a threefold-degenerate lowest excitation with $S^z_{\text{total}}=0,\pm1$ for the SF state. The phase transition is actually caused by the level crossing of the first-excited state. Tian *et al.*[41] also pointed this out. They found that when level crossing of the ground state is absent, a quantum phase transition is usually caused by a reconstruction of low-excitation spectrum of the system. Therefore, the SDFE can be used to indicate the phase-transition point; however, when the system size N increases, the energy gap between the ground state and the first-excited state rapidly decreases and finally vanished (degenerated) in the thermodynamic limit. Consequently the absolute value of the extremum in the SDFE decreases and may vanish in the infinite-size case.

In addition, the boundary of the ferrimagnetic phase in Fig. 4 is not one clear curve but consists of the curves marked by red arrows, and there is a sharp drop point in the SDFE near $J_1/J_2=1.0$ and $J_3/J_2=0.37$. Can all these drop regions be regarded as new quantum phase-transition points? To answer this question, let us turn to the energy spectrum of the system.

We present the energy spectrums E as functions of J_3/J_2 for two specific transects at $J_1/J_2=1.0$ and $J_1/J_2=1.25$ for $N=12$ in Figs. 7(a) and 7(b) and their SDFEs are plotted in Figs. 7(c) and 7(d), respectively. There are four critical points numbered in Fig. 7(b)—three level-crossing points and a two-level degenerated region beginning at $J_3/J_2=0.84$—for the first-excited state. The drops and the peak in Fig. 7(d) correspond to these points. The drop point 1 and the peak in Fig. 7(d) are caused by the level crossings of the first-excited state with the third excited level and the ground state, respectively; therefore drop 1 is related to the SF-D phase-transition point and the peak is a precursor of the

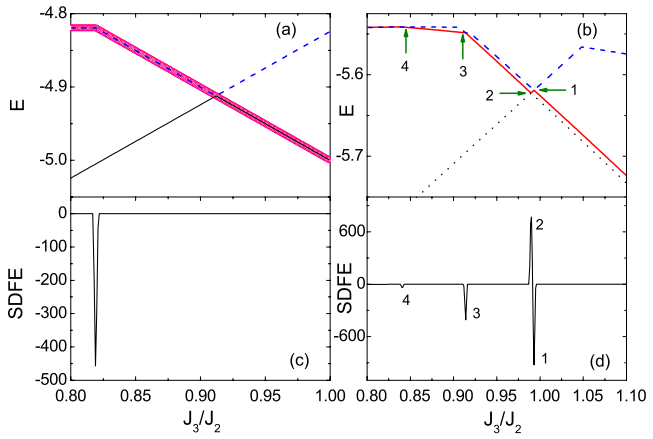

FIG. 7. (Color online) The lowest three energy levels of the DDC model with $N=12$ for $J_1/J_2=$(a) 1.0 and (b) 1.25 as a function of J_3/J_2. (c) and (d) are their corresponding second derivatives of the first-excited energy.

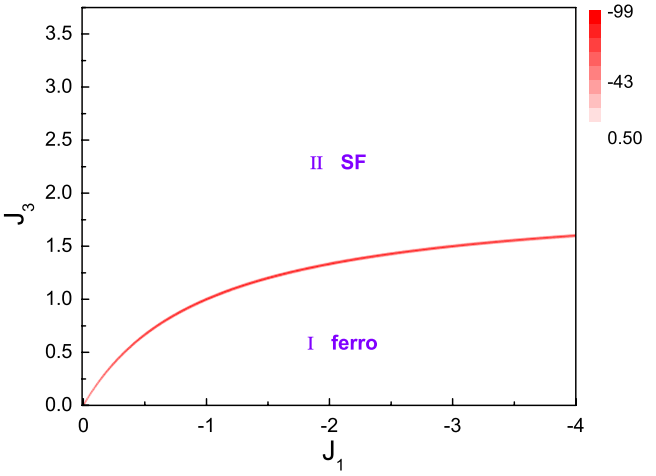

FIG. 8. (Color online) Contour map of the SDGE with respect to J_3 for the ferromagnetic frustrated DDC model with $N=12$ and $J_2=-1.0$ on the J_1-J_3 plane.

ferri-SF phase transition. Because they are so close to each other that instead of two curves, they make a wide-line-like display, as signaled by curve 1 in Fig. 4. Meanwhile, with J_1/J_2 approaching to 1.0, the distance between the two-level-crossing points becomes smaller and the ground state and the first excitation degenerate for $J_3/J_2>0.99$ at $J_1/J_2=1.0$, making the two-level crossings vanish, as shown in Fig. 7(a); therefore the wide curve 1 becomes narrower as J_3/J_2 decreases and vanishes near $J_1/J_2=1.0$. The drops 3 and 4 in Fig. 7(d) correspond to the curves 2 and 3 in Fig. 4, respectively, and the sharp drop point near $J_1/J_2=1.0$ and $J_3/J_2=0.37$ is due to the energy level crossing of the first excitation with higher energy levels. But these drops are not caused by the energy-level crossing of the threefold-degenerate excitation and the singlet excitation as mentioned above; therefore it cannot be regarded as precursors of the quantum critical point.

Now, we can say that the SDFE can be exploited as a useful tool to identify some kinds of continuous QPTs, for which the SDGE is ineffective, such as the BKT-type QPT, but is not always a good indicator of QPTs.

We then focused on the ferromagnetic frustrated case ($J_1,J_2<0$ and $J_3>0$). We keep $J_2=-1.0$ unchanged. The contour map of the SDGE with respect to J_3 in the plane of J_1-J_3 is shown in Fig. 8. The sharp drops in the SDGEs separate the diagram into two parts (I and II). We can confirm that the region I corresponds to a ferromagnetic phase and the region II corresponds to the SF one. This can be understood from the physical properties keeping J_1 unchanged, when J_3 is small the ferromagnetic interactions J_1 and J_2 are dominant, making the spins a ferromagnetic arrangement, while with the increase of J_3, dimers between the spins connected by J_3 are formed and due to the frustration effect, the system changes into the SF state.

We also calculate the SDFE for the ferromagnetic frustrated DDC case, but the results show no more new phase than the SDGE results. There is no spin-gapped D phase as in the antiferromagnetic frustrated case; therefore we do not show the results here.

B. Trimerized case

When $J_2=0$, the DDC model becomes the trimerized Heisenberg chain model. The SDGEs with respect to J_3 and J_1 for this case are plotted in Figs. 9(a) and 9(b), respectively. We work in units where J_1 and J_3 are dimensionless. As shown in Fig. 9(a), there is a phase-transition line indicated by the sharp drops in the SDGEs along $J_3=0.0$ through all the AF and F interaction regions of J_3; while a phase-transition line along $J_1=0.0$ appears only in $J_3<0$ region, i.e., in the J_3 being the ferromagnetic interaction region in Fig. 9(b). The sharp drops in Fig. 9 indicate some kinds of phase transitions there.

These quantum phases could be identified by analyzing the spin arrangement conditions. We plot the schematic spin arrangements for different conditions in Fig. 10. It shows that when both J_1 and J_3 are ferromagnetic interactions (the F-F-F case), all the spins arrange in the same direction. The magnitude S_{total} of the total spin $\boldsymbol{S}_{\text{total}}$ is $N/2$, which corresponds to a ferromagnetic state (ferro); while $J_1=J_{\text{AF}}$ and $J_3=J_{\text{F}}$ (the AF-AF-F case), because the total spin in different directions are different, the system falls into a ferrimagnetic state (ferri) with $S_{\text{total}}=N/6$. If $J_1,J_3=J_{\text{AF}}$ (the AF-AF-AF case), each spin is antiparallel to its neighbor and the system displays a typical antiferromagnetic state (antiferro) with $S_{\text{total}}=0$; when $J_1=J_{\text{F}}$ and $J_3=J_{\text{AF}}$ (the F-F-AF case), the

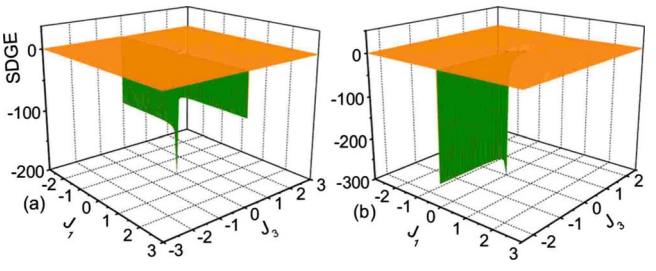

FIG. 9. (Color online) SDGE of the trimerized model for $N=12$ and δJ_1, $\delta J_3=0.01$ with respect to (a) J_3 and (b) J_1. We work in units where J_1 and J_3 are dimensionless.

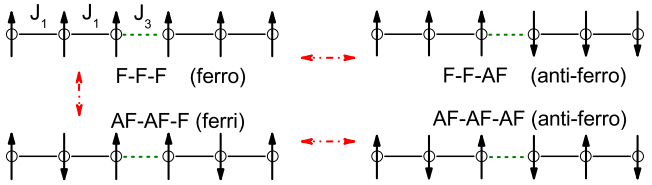

FIG. 10. (Color online) Sketch of spin arrangement for the trimerized spin chain, where F and AF present different interactions of J_1 and J_3. The red bidirectional arrows indicate the quantum phase transitions.

spins connected by J_1 can be regarded as a $S=3/2$ cluster and all the clusters display an antiferromagnetic arrangement, which also corresponds to an antiferromagnetic spin chain. Therefore, three phases exist for the trimerized chain. As J_3 changes from ferromagnetic to antiferromagnetic, the system would change from the ferrostate to the antiferrostate when $J_1=J_F$; while the system would change from the ferristate phase to the antiferrostate when $J_1=J_{AF}$, as indicated in Fig. 9(a) and sketched out in Fig. 10. The sharp drops in Fig. 9(b) indicate the ferro-ferri phase transition; while, because the system is an antiferromagnetic spin chain for both ferromagnetic and antiferromagnetic J_1 when $J_3=J_{AF}$, there is no phase transition at all, which results in the smooth changing behavior of the SDGEs in the $J_3>0$ region of Fig. 9(b). The bidirectional arrows in Fig. 10 indicate these phase transitions of the trimerized chain case.

IV. THERMAL ENTANGLEMENT ENTROPY AND QPTS

The above results are all about finite-size systems. We now calculate the finite-temperature entanglement entropy E_t by exploiting the TMRG method to explore the QPTs of the DDC model in the thermodynamic limit. The method and the calculated details have been introduced in Sec. II.

We choose a special transect $J_1/J_2=1.0$ of the antiferromagnetic frustrated DDC model, i.e., the diamond-chain model, to verify the validity of our finite-temperature entanglement method in identifying QPTs. The E_t as a function of J_3/J_2 is shown in Fig. 11. There are two drops of E_t near $J_3/J_2=2.0$ and 1.0, respectively. The two drops become sharper and sharper around two points marked A and B in Fig. 11(a) with temperature decrease and clearly divide the low-temperature curve into three parts. It seems that there

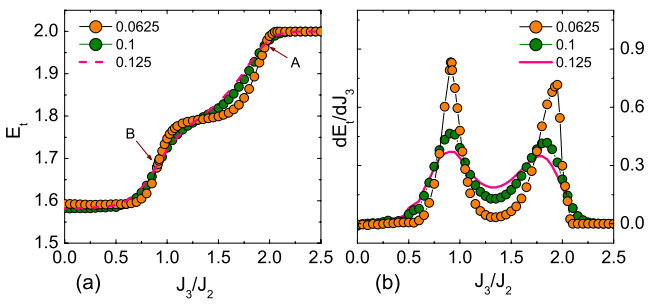

FIG. 11. (Color online) (a) The thermal entanglement E_t of the antiferromagnetic DDC model as a function of J_3/J_2 at $J_1/J_2=1.0$ for different temperatures T/J_2 and (b) their J_3 derivatives.

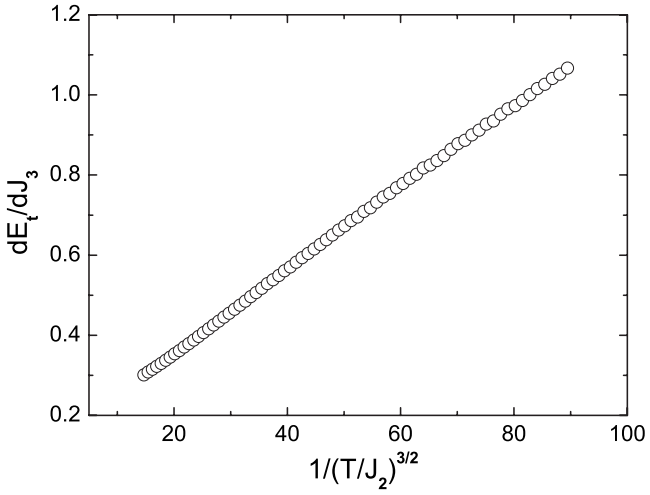

FIG. 12. The temperature-scaling behavior of the value of dE_t/dJ_3 near the critical point $J_3/J_2=0.909$ for the antiferromagnetic DDC model at $J_1/J_2=1.0$.

will be a straight drop at these two points in the $T=0$ limit. Points A and B correspond to $J_3/J_2=0.91$ and 1.95, respectively, which are quite close to the two phase-transition points for the diamond model. The E_t curve here sketches out the three phases of the diamond chain. Meanwhile, we plot the J_3 derivative of E_t in Fig. 11(b). We note that the peaks around the critical points become more pronounced as temperature decreases. The value of the peak at $J_3/J_2=0.91$ scales as (see Fig. 12, where $m=120$ states are retained during the TMRG calculations)

$$\left.\frac{dE_t}{dJ_3}\right|_{J_1/J_2=0.91} = 0.0103/(T/J_2)^{3/2} + \text{const}, \tag{8}$$

and it is expected to be divergent in the $T=0$ limit. Here, the peaks of low-temperature curve ($T/J_2=0.0625$) clearly indicate the QPTs, which happen at zero temperature.

In addition, we also calculate the two-site thermal entanglement E_t for the ferromagnetic frustrated case and the trimerized chain model shown in Fig. 13. Figure 13(a) shows

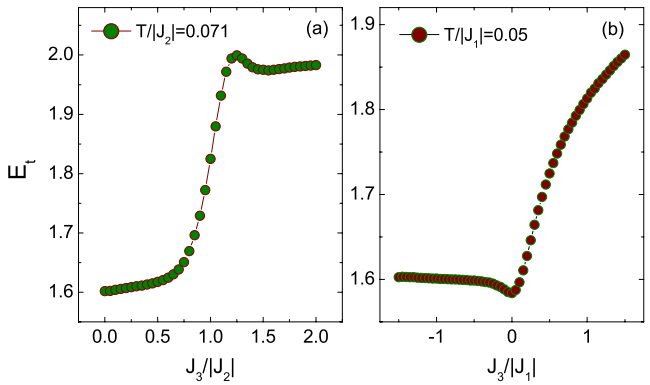

FIG. 13. (Color online) (a) E_t of the ferromagnetic frustrated DDC model as a function of $J_3/|J_2|$ at $J_1/|J_2|=-1.5$ and $T/|J_2|=0.071$. (b) E_t of the trimerized chain model with $J_1=-1.0$ as a function of $J_3/|J_1|$ at $T/|J_1|=0.05$.

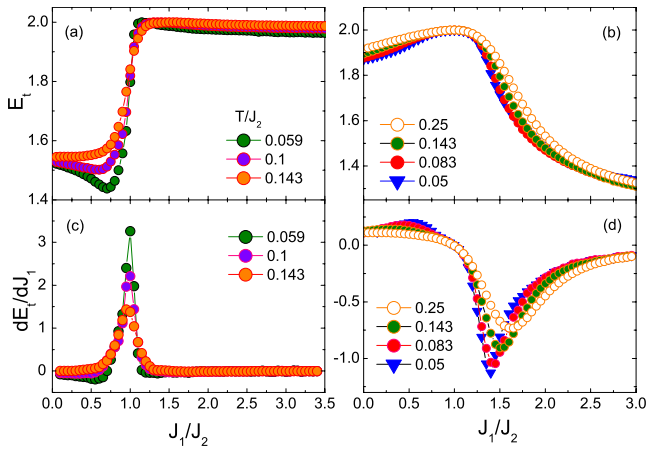

FIG. 14. (Color online) E_t of the antiferromagnetic frustrated DDC model as a function of J_1/J_2 under different temperatures at (a) $J_3/J_2=1.5$ and (b) $J_3/J_2=3.0$. (c) and (d) are their J_1 derivatives, respectively.

the E_t results for the ferromagnetic frustrated case as a function of $J_3/|J_2|$ at $J_1/|J_2|=-1.5$ and $T/|J_2|=0.071$. Instead of a sharp drop, the E_t curve shows a maximum at the phase-transition point $J_3/|J_2|\approx 1.25$. This data is close to that of the SDGE result shown in Fig. 8. The E_t as a function of $J_3/|J_1|$ for the trimerized chain at $J_1=-1.0$ and $T/J_1=0.05$ is plotted in Fig. 13(b). We have calculated and analyzed that an antiferro-ferro QPT exists at $J_3=0$ for the trimerized chain model when $J_1=J_F$. The minimum of our E_t results in Fig. 13(b) clearly marked the transition point. All these results indicate the feasible role of E_t in identifying QPTs. The two-site thermal entanglement E_t would show sharp drop or extremum at the quantum phase-transition points, and the difference of the sharp drop and the extremum displayed by E_t may reflect the difference of phase-transition types.

Now let us return to the question in Sec. III on whether the minima in Fig. 3 could be regarded as a precursor of QPT. We plot the E_t as a function of J_1/J_2 for $J_3/J_2=1.5$ and its first-order J_3 derivative in Figs. 14(a) and 14(c), respectively. Both the drops in the E_t curves and the peaks in the dE_t/dJ_3 curves become more pronounced as temperature decreases. The sharp drops and the peaks reflect the existence of a QPT at the vicinity of $J_1/J_2\approx 1.0$ in the D phase region. We also calculate the E_t and its J_1 derivatives as a function of J_1/J_2 at $J_3/J_2=3.0$, i.e., at the SF region [Figs. 14(b) and 14(d)]. The two-site thermal entanglement E_t reaches its maximum value at $J_1/J_2=1.0$ and its J_1 derivative dE_t/dJ_1 shows a minimum which is pronounced and toward the side of $J_1/J_2=1.0$ with decreasing temperature. These anomalies also indicate that there might exist a QPT at the vicinity of $J_1/J_2\approx 1.0$ in the SF phase region, as predicted in Sec. III. The main reason for this may be that when $J_1=J_2$, there is more symmetric structure. In the $0.909<J_3/J_2<2.0$ region, it is the tetramer-dimer phase. As J_3/J_2 further increases, the interaction of J_3 becomes more prominent and the tetramer structure is broken. The system forms the dimer-monomer state;[30] whereas the symmetric structure is broken and some effective interactions are formed when $J_1\neq J_2$, resulting in the dimer and SF phases. The dramatic changes in the SDGE and the E_t at the critical vicinity of $J_1/J_2\approx 1.0$ could be regarded as the reflection of the existence of the tetramer-dimer and dimer-monomer phases.

V. SUMMARY

In summary, we obtained the expression of the SDGE and showed its same origin with the fidelity susceptibility in terms of the quantum perturbation theory. By using the exact diagonalization method, we calculated the SDGE of the DDC model for finite-size systems and obtained the phase diagrams for the antiferromagnetic frustrated, ferromagnetic frustrated, and trimerized cases. Except the SF-D phase transition, the critical regions indicated by the abrupt drops in the antiferromagnetic case are consistent with those results in Ref. 31, while the SF-D phase transition can be indicated by the SDFE of the system. Our results show that the SDGE is a good indicator of QPTs in most cases. But for those continuous phase transition induced by the low-lying excited states, we may need the help from the SDFE. Our SDFE results for the antiferromagnetic frustrated case clearly indicate the SF-D phase transition. However, the absolute value of the sharp drop decreases as the system size increases for the BKT-type phase transition (in DDC and J_1-J_2 models) and might vanish in the thermodynamic limit because of the energy-level degeneracy. Meanwhile, not all the sharp drops in SDFEs, which are caused by the low-lying level crossing, could be regarded as indicators of QPTs. Thus, the SDFE might only be used as an assistant tool to investigate QPTs. In addition, we showed that the two-site thermal entanglement calculated by TMRG method can be exploited as a useful tool to investigate QPTs of a system in the thermodynamic limit, and we detected the TD state in the D phase and the DM state in the SF phase by this method.

ACKNOWLEDGMENTS

This work was supported by the National Basic Research Program of China (973 Program) under Grant No. G2009CB929300 and the National Natural Science Foundation of China under Grants No. 60521001 and No. 60776061.

[1] S. Sachdev, *Quantum Phase Transition* (Cambridge University Press, Cambridge, UK, 1999).
[2] F. Plastina and T. J. G. Apollaro, Phys. Rev. Lett. **99**, 177210 (2007).
[3] C. Cormick and J. P. Paz, Phys. Rev. A **78**, 012357 (2008).
[4] N. D. Mathur, F. M. Grosche, S. R. Julian, I. R. Walker, D. M. Freye, R. K. W. Haselwimmer, and G. G. Lonzarich, Nature (London) **394**, 39 (1998).

[5] A. Osterloh, Luigi, Amico, G. Falci, and Rosario Fazio, Nature (London) **416**, 608 (2002).
[6] S. J. Gu, S. S. Deng, Y. Q. Li, and H. Q. Lin, Phys. Rev. Lett. **93**, 086402 (2004).
[7] L. A. Wu, M. S. Sarandy, and D. A. Lidar, Phys. Rev. Lett. **93**, 250404 (2004).
[8] A. Anfossi, P. Giorda, A. Montorsi, and F. Traversa, Phys. Rev. Lett. **95**, 056402 (2005).
[9] S. S. Deng, S. J. Gu, and H. Q. Lin, Phys. Rev. B **74**, 045103 (2006).
[10] Ö. Legeza and J. Sólyom, Phys. Rev. Lett. **96**, 116401 (2006); Ö. Legeza, K. Buchta, and J. Sólyom, Phys. Rev. B **73**, 165124 (2006).
[11] S. Q. Su, J. L. Song, and S. J. Gu, Phys. Rev. A **74**, 032308 (2006).
[12] P. Zanardi and N. Paunkovic, Phys. Rev. E **74**, 031123 (2006); P. Zanardi, M. Cozzini, and P. Giorda, J. Stat. Mech.: Theory Exp. (2007) L02002; P. Zanardi, H. T. Quan, X. G. Wang, and C. P. Sun, Phys. Rev. A **75**, 032109 (2007).
[13] Y. C. Tzeng and M. F. Yang, Phys. Rev. A **77**, 012311 (2008).
[14] S. Chen, L. Wang, S. J. Gu, and Y. Wang, Phys. Rev. E **76**, 061108 (2007).
[15] S. Chen, L. Wang, Y. Hao, and Y. Wang, Phys. Rev. A **77**, 032111 (2008).
[16] S. J. Gu, H. M. Kwok, W. Q. Ning, and H. Q. Lin, Phys. Rev. B **77**, 245109 (2008).
[17] W. L. You, Y. W. Li, and S. J. Gu, Phys. Rev. E **76**, 022101 (2007).
[18] P. Buonsante and A. Vezzani, Phys. Rev. Lett. **98**, 110601 (2007).
[19] M. Cozzini, P. Giorda, and P. Zanardi, Phys. Rev. B **75**, 014439 (2007); M. Cozzini, R. Ionicioiu, and P. Zanardi, *ibid.* **76**, 104420 (2007).
[20] G. Misugich and C. Lhuillier, in *Frustrated Spin Systems*, edited by H. T. Diep (World Scientific, Singapore, 2004).
[21] H. Kikuchi, Y. Fujii, M. Chiba, S. Mitsudo, T. Idehara, T. Tonegawa, K. Okamoto, T. Sakai, T. Kuwai, and H. Ohta, Phys. Rev. Lett. **94**, 227201 (2005); **97**, 089702 (2006).
[22] H. H. Fu, K. L. Yao, and Z. L. Liu, Phys. Rev. B **73**, 104454 (2006).
[23] I. A. Kiseleva, L. P. Ogorodova, L. V. Melchakova, M. R. Bisengalieva, and N. S. Becturganov, Phys. Chem. Miner. **19**, 322 (1992).
[24] K. L. Yao, Q. M. Liu, and Z. L. Liu, Phys. Rev. B **70**, 224430 (2004).
[25] A. Honecker and A. Läuchli, Phys. Rev. B **63**, 174407 (2001).
[26] Y. C. Li, J. Appl. Phys. **102**, 113907 (2007).
[27] B. Gu and G. Su, Phys. Rev. B **75**, 174437 (2007).
[28] Z. Y. Sun, K. L. Yao, W. Yao, D. H. Zhang, and Z. L. Liu, Phys. Rev. B **77**, 014416 (2008).
[29] M. S. S. Pereira, F. A. B. F. de Moura, and M. L. Lyra, Phys. Rev. B **77**, 024402 (2008).
[30] K. Takano, K. Kubo, and H. Sakamoto, J. Phys.: Condens. Matter **8**, 6405 (1996).
[31] K. Okamoto, T. Tonegawa, Y. Takahashi, and M. Kaburagi, J. Phys.: Condens. Matter **11**, 10485 (1999); K. Okamoto, T. Tonegawa, and M. Kaburagi, *ibid.* **15**, 5979 (2003).
[32] T. Tonegawa, K. Okamoto, T. Hikihara, Y. Takahashi, and M. Kaburagi, J. Phys. Soc. Jpn. (Suppl. A) **69**, 332 (2000); J. Phys. Chem. Solids **62**, 125 (2001).
[33] K. Sano and K. Takano, J. Phys. Soc. Jpn. **69**, 2710 (2000).
[34] H. T. Wang, J. Phys.: Condens. Matter **14**, 8033 (2002).
[35] R. J. Bursill, T. Xiang, and G. A. Gehring, J. Phys.: Condens. Matter **8**, L583 (1996); X. Wang and T. Xiang, Phys. Rev. B **56**, 5061 (1997).
[36] T. Xiang and X. Wang, in *Density-Matrix Renormalization: A New Numerical Method in Physics*, edited by I. Peschel, X. Wang, M. Kaulke, and K. Hallberg (Springer, New York, 1999), pp. 149–172; U. Schollwock, Rev. Mod. Phys. **77**, 259 (2005).
[37] O. F. Syljuåsen, Phys. Rev. A **68**, 060301(R) (2003).
[38] V. L. Beresinskii, Sov. Phys. JETP **32**, 493 (1971).
[39] J. M. Kosterlitz and D. J. Thouless, J. Phys. C **6**, 1181 (1973); J. M. Kosterlitz, *ibid.* **7**, 1046 (1974).
[40] C. N. Yang and C. P. Yang, Phys. Rev. **150**, 321 (1966); J. D. Cloizeaux and M. Gaudin, J. Math. Phys. **7**, 1384 (1966).
[41] G. S. Tian and H. Q. Lin, Phys. Rev. B **67**, 245105 (2003).